Catalysis Science & Technology

Deoxydehydration of 1,4-anhydroerythritol over anatase TiO2(101)-supported ReOx and MoOx

Journal:	*Catalysis Science & Technology*
Manuscript ID	CY-ART-03-2020-000434.R1
Article Type:	Paper
Date Submitted by the Author:	04-May-2020
Complete List of Authors:	Xi, Yongjie; University of South Carolina, Chemical Engineering Lauterbach, Jochen; University of South Carolina, Chemical Engineering Pagan Torres, Yomaira; University of Puerto Rico Mayaguez Heyden, Andreas; University of South Carolina, Chemical Engineering

Deoxydehydration of 1,4-anhydroerythritol over anatase TiO_2(101)-supported ReO_x and MoO_x

Yongjie Xi[#], Jochen Lauterbach[#], Yomaira Pagan-Torres[$] and Andreas Heyden[#,*]

[#] Department of Chemical Engineering, University of South Carolina, 301 South Main Street, Columbia, South Carolina 29208, United States

[$]Department of Chemical Engineering, University of Puerto Rico-Mayaguez Campus, Mayaguez, Puerto Rico 006814-9000, United States

Abstract:

Heterogeneously catalyzed deoxydehydration (DODH) ordinarily occurs over relatively costly oxide supported ReO_x sites and is an effective process for the removal of vicinal OH groups that are common in biomass-derived chemicals. Here, through first-principles calculations, we investigate the DODH of 1,4-anhydroerythritol over anatase TiO_2(101)-supported ReO_x and MoO_x. The atomistic structures of ReO_x and MoO_x under typical reaction conditions were identified with constrained thermodynamics calculations as ReO_2(2O)/6H-TiO_2 and MoO(2O)/3H-TiO_2, respectively. The calculated energy profile and developed microkinetic reaction model suggest that both ReO_2(2O)/6H-TiO_2 and MoO(2O)/3H-TiO_2 exhibit a relatively low DODH activity at 413 K. However, at higher temperatures such as 473 K, MoO(2O)/TiO_2(101) was found to exhibit a reasonably high catalytic activity similar to ReO_2(2O)/6H-TiO_2, consistent with a recent experimental study. Mechanistically, the first O-H bond cleavage of 1,4-anhydroerythritol and the dihydrofuran extrusion were found to be the rate-controlling steps for the reaction over ReO_2(2O)/6H-TiO_2 and MoO(2O)/3H-TiO_2, respectively. Thus, this study clarifies the mechanism of the DODH over oxide-supported catalysts and provides meaningful insight into the design of low-cost DODH catalysts.

1. Introduction

The conversion of renewable biomass into fuels and value-added chemicals is a promising way to mitigate overdependence on petroleum and to achieve sustainability.[1-4] Biomass-derived chemicals are typically oxygen-rich, making it necessary to reduce the oxygen content to valorize biomass. Various deoxygenation processes have been developed, including the DODH process whereby a vicinal alcohol is converted to one C=C double bond. This process has been found particularly efficient for removal of multiple OH groups.[5, 6] The first homogeneous DODH catalyst is a $(C_5Me_5)ReO_3$ complex and was reported in 1996.[7] Other organometallic catalysts were also explored as DODH catalysts, among them commercially available methyltrioxorhenium (MTO) is one of those catalysts that has been explored most extensively.[8] Heterogeneous DODH catalysts were developed recently. The first catalyst was a carbon-supported perrhenate, which was flawed by the problem of catalyst leaching into the solvent and fast activity loss.[9] Re species supported on ceria exhibit a higher level of stability than those that are carbon supported. DODH catalyzed by ReO_x−Pd/CeO_2[10, 11] or ReO_x−Au/CeO_2[12, 13] was found to exhibit high activity and selectivity towards desired products, where the Pd or Au promoter was used to catalyze the H_2 dissociation that is indispensable for the regeneration of the catalyst.

The reported DODH catalysts feature a metal-oxo compound. Mechanistically, the first O-H cleavage takes place upon H migration to the oxygen of the metal-oxo and the concomitant binding between the reactant O and the metal center. The second OH of a diol reactant reacts with the formed OH group bonded with the metal-oxo, forming a diolate species and a water molecule. Removal of the alkene leaves an additional oxygen atom on the catalyst and typically

involves overcoming a significant energy barrier.[5, 14] To regenerate the catalyst, the high valent species has to be reduced, which can be achieved with H_2,[8] PPh_3,[7] Na_2SO_3,[15] and alcohols.[16] Computational studies have been performed to understand the mechanism of homogeneous DODH reactions.[17, 18] Recently, we reported a comprehensive mechanistic study of the heterogeneous catalyzed DODH over ReO−Pd/CeO_2. Pd was found to catalyze the hydrogen dissociation and spillover onto the CeO_2 support, as well as modify the oxidation state of Re from +6 to +7 when it is adsorbed near ReO, thus increasing the DODH activity of ReO.[14]

While the majority of DODH catalysts are based on Re, inexpensive alternatives such as Mo-[19] and V-catalysts[20] were also explored. Apart from ceria supported DODH catalysts, titania was also examined as support for metal-oxo DODH catalysts.[19, 21] Unlike the carbon supported ReO_x catalyst which undergoes catalyst leaching into the solvent, a TiO_2-supported catalyst was found to exhibit improved stability. In a comparative study by Palkovits et. al., the ReO_x species exhibits comparable catalytic activities in the presence of different supports with 1-octanol as hydrogen source and the TiO_2-supported ReO_x exhibits the highest stability.[21] Another catalyst screening process by Tomishige et. al. suggests that CeO_2 supported ReO_x exhibits the highest activity among the investigated oxide supports when using H_2 gas as reductant while the activity of ReO_x/TiO_2 is relatively poor at 413K.[10] In contrast, anatase TiO_2-supported MoO_x was found to be active for the catalytic DODH reaction of cis-1,4-anhydroerythritol with 3-octanol as reductant.[19] Similarly, in another recent study anatase TiO_2-supported MoO_x was found to catalyze the DODH of 1,2-decane diol with H_2 as the reductant.[22] Therefore, it is intriguing to understand the different catalytic properties of TiO_2-supported ReO_x and MoO_x for the DODH reaction.

In the present study, we used first principles calculations to better understand the mechanism of DODH reactions catalyzed by ReO_x or MoO_x when bonded to a anatase TiO_2 support. H_2 is used as a reductant to regenerate the catalysts and the most stable (101) anatase facet was adopted to construct the atomistic model. Constrained thermodynamics calculations were performed to determine the atomistic structure of ReO_x/TiO_2 and MoO_x/TiO_2 under experimental reaction conditions. The DODH of cis-1,4-anhydroerythritol (AE) into dihydrofuran (DHF) was used as a probe reaction.[11, 19] The energy pathways were determined through first principles calculations, followed by microkinetic modeling, which provides further insight into the reaction mechanism and rate controlling steps.

2. Computational methods and models

2.1 First principles methods

First-principles calculations were performed using periodic density functional theory (DFT), as implemented in the Vienna Ab initio Simulation Package (VASP 5.4.4).[23, 24] The spin-polarized generalized gradient approximation (GGA) with the PBE functional[25] was used to treat exchange−correlation effects. A plane wave basis set with a cutoff energy of 400 eV was selected to describe the valence electrons. The electron−ion interactions were described by the projector augmented wave (PAW)[26, 27] method. An effective Hubbard U value of 3.5 eV was used to describe the strong on-site Coulomb repulsion of the Ti 3d electrons, following previous research.[28] The Brillouin zone integration was performed with a 2×2×1 Monkhorst−Pack[29] (MP) k-mesh and Gaussian smearing (σ=0.1 eV). We used Grimme's DFT-D3[30] scheme to include the van der Waals interactions semi-empirically. The SCF and force

convergence criteria for structural optimization were set to 1×10^{-5} eV and 0.01 eV/Å, respectively. The climbing image nudged elastic band (CI-NEB)[31] and dimer methods[32, 33] were used to optimize the transition state structures. The force convergence criterion for transition state optimization was set to be 0.03 eV/Å. Computational details on the calculation of free energies for surface and gas species are presented in the ESI.

2.2 Atomistic model

A (2×3) supercell slab model with four O-Ti-O trilayer anatase TiO_2(101) was used to describe the TiO_2 slab and neighboring slabs were separated by a 15 Å vacuum slab. Under a typical experimental condition of 413 K and a H_2 partial pressure of 80 bar,[11] the TiO_2(101) surface can be terminated with hydrogen. Hydrogen atoms are added to the oxygen at the topmost layer, which is found to be the most stable adsorption site for hydrogen. We performed constrained ab initio thermodynamics calculations to determine the structure of TiO_2(101) at various temperatures. The free energy of hydrogen adsorption (H_2, 80 bar) is calculated as $G_{ads}(H)= G(TiO_2H_x)-G(TiO_2)-0.5 \times G(H_2)$, where x is the number of adsorbed hydrogen atoms which is in the range of 1-6 for a (2×3) supercell (Fig. 1a). Since the stability of the surfaces with different hydrogen coverage is similar, we initially employed a fully-hydrogenated TiO_2(101) model to construct the atomistic model of ReO_x/TiO_2 and MoO_x/TiO_2 (Fig. 1b). We found that Re(2O) or Mo(2O) can be stabilized on the fully-hydrogenated TiO_2(101) surface (6H-TiO_2(101)) with the Re or Mo being bridged to TiO_2(101) by two oxygen atoms. The free energy of Re(2O) adsorption is calculated as $G_{ads}=[G(TiO_2\text{-}Re(2O)-E(Re)-2G(H_2O)+2G(H_2)]$ and the free energy of Mo(2O) adsorption is calculated in the same vein. The adsorption free energies of Re(2O) or Mo(2O) were calculated to be -4.04 and -4.01 eV (413K; H_2: 80bar; H_2O:

0.08 bar), respectively (Fig. 1c, d). Repeated attempts were also made to calculate the structures with the Re or Mo directly being bonded to the TiO_2(101). However, if two oxygen atoms are added above the Re or Mo atoms, these structures transformed to the oxygen-bridged structures after optimization. In other words, a Re or Mo atom can be anchored by two oxygen atoms on a hydrogenated TiO_2(101) surface.

Based on Re(2O)/TiO_2(101) and Mo(2O)/TiO_2(101), we also examined the possibility of whether additional O or OH can be accommodated on Re or Mo under reaction conditions at various hydrogen coverage. The adsorption of OH is considered due to the presence of H_2O under reaction conditions. Therefore, $O_a(OH)_b$ species are allowed to adsorb on Re(2O)/TiO_2(101) or Mo(2O)/TiO_2(101). Except for MoO_3, an $O_a(OH)_b$ species with a+b no greater than 3 can be added. MoO_3 is not further discussed since it is not well-stabilized by Mo(2O)/TiO_2(101). Next, we preformed constrained ab initio thermodynamics calculations to examine the stability of $ReO_a(OH)_b$(2O)/$MoO_a(OH)_b$(2O) on an anatase TiO_2 surface at various H coverage (1H-6H) using Re(2O)/6H-TiO_2(101) and Mo(2O)/6H-TiO_2(101) as reference states, respectively. In Fig. 2, we present the free energies of the two most stable configurations at various hydrogen coverage while the complete free energy diagrams are presented in Figs. S1-S12. The optimized configurations of $ReO_a(OH)_b$(2O)/6H-TiO_2(101) and $MoO_a(OH)_b$(2O)/6H-TiO_2(101) are presented in Fig. S13 while all configurations are available in the ESI as coordinate files. Overall, the TiO_2(101) surface with preadsorbed Re(2O) can accommodate more oxygen species than that of Mo(2O) at the same hydrogen coverage. The most stable species of $ReO_a(OH)_b$(2O) and $MoO_a(OH)_b$(2O) were identified to be ReO_2(2O) on a fully-hydrogenated TiO_2(101) surface and MoO(2O) on TiO_2(101) with three adsorbed

hydrogen atoms, respectively. By using spin density plots, the oxidation state of Re for 6H-ReO_2(2O) and Mo for 3H-MoO (2O) were determined to be +7 and +6, respectively (Fig. 3). The assignment of oxidation state is based on the number of Ti^{3+} that are reduced from Ti^{4+} by H, ReO_2(2O) and MoO(2O). Each H can donate one electron to the TiO_2(101) support, therefore ReO_2(2O) and MoO_2(2O) have a positive charge of 1 and 0, respectively.

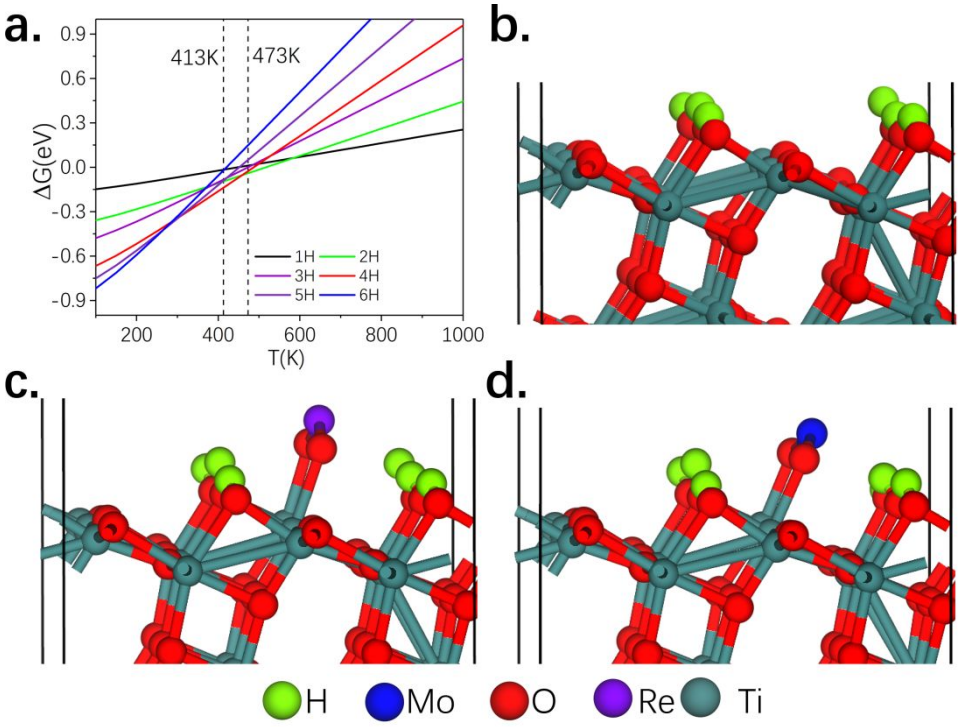

Fig. 1a. Results from constrained ab initio thermodynamics calculations of hydrogen adsorption on (2×3) anatase TiO_2(101). The H_2 partial pressure is 80 bar. **b.** Configuration of the fully hydrogenated (2×3) anatase TiO_2(101). **c.** and **d.** Adsorption of ReO_2 and MoO_2 on fully hydrogenated (2×3) anatase TiO_2(101), respectively.

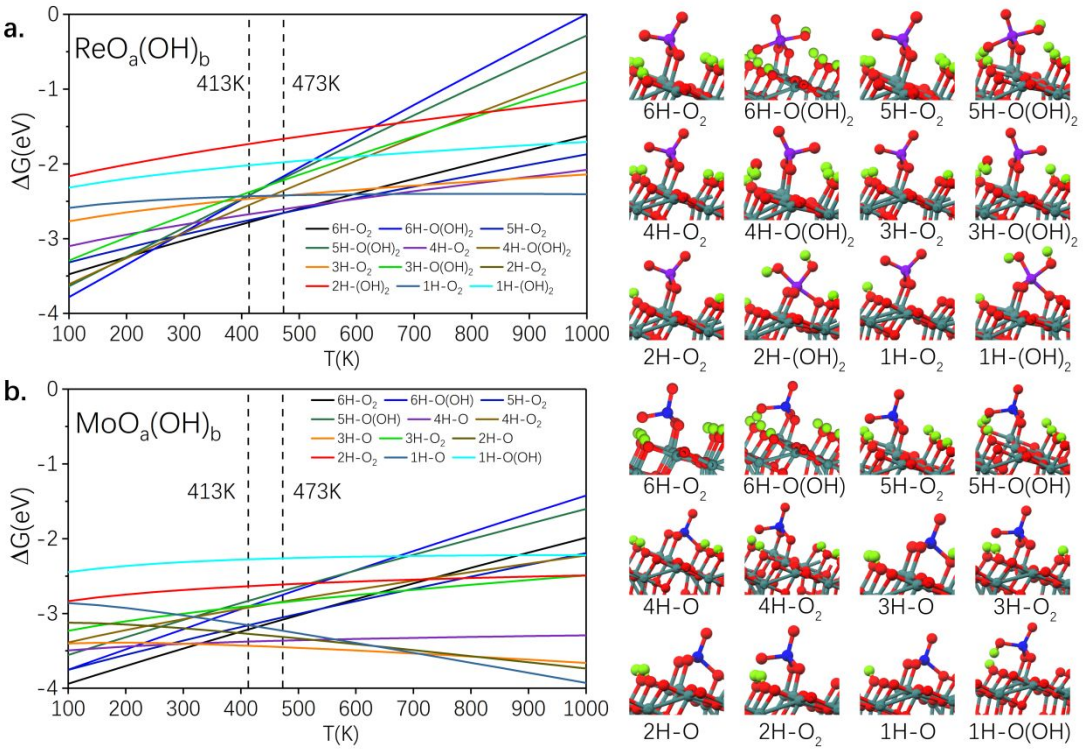

Fig. 2 The Gibbs free energies of selected (**a**) $ReO_a(OH)_b(2O)$ and (**b**) $MoO_a(OH)_b(2O)$ species adsorbed on $TiO_2(101)$ at various hydrogen coverages (1H-6H) with a hydrogen partial pressure of 80 bar and water partial pressure of 0.08 bar, respectively. Note that for 3H-$O(OH)_2$ and 4H-$O(OH)_2$ of $ReO_a(OH)_b$, a H_2O molecule is formed after optimization. Re(2O)/6H-$TiO_2(101)$ and Mo(2O)/6H-$TiO_2(101)$ are set to be the reference states, respectively. The free energy of $ReO_a(OH)_b(2O)$ and $MoO_a(OH)_b(2O)$ relative to Re(2O)/6H-$TiO_2(101)$ and Mo(2O)/6H-$TiO_2(101)$ are balanced by adding H_2 and H_2O, e.g., G[$ReO_2(2O)$] = G[Re(2O)] + 2G(H_2O)-2G(H_2). For brevity, Re(2O) and Mo(2O) are regarded to be pre-adsorbed onto $TiO_2(101)$ and denoted as Re and Mo in **a** and **b**; the number of hydrogen atoms adsorbed on $TiO_2(101)$ are added before the $O_a(OH)_b$ notation.

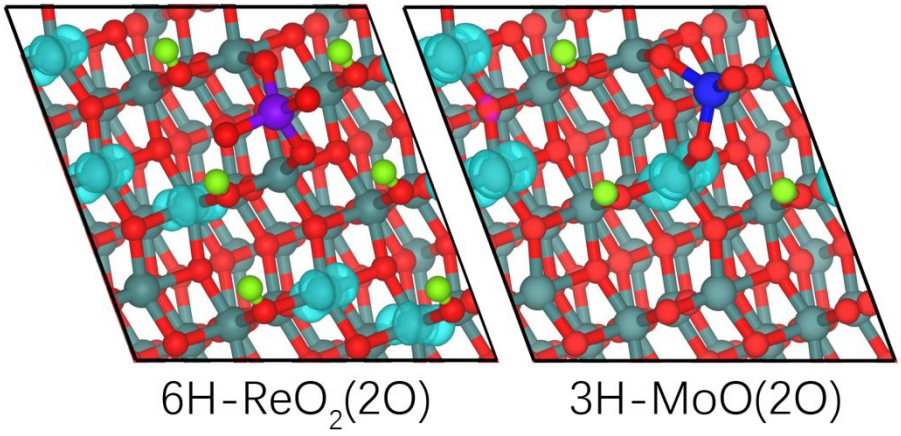

Fig. 3 Spin density of 6H-$ReO_2(2O)$ and 3H-MoO(2O) supported on $TiO_2(101)$. There are 5 and 3 Ti^{3+} ions in the 6H-$ReO_2(2O)$ and 3H-MoO (2O) models, respectively. The isosurface value is 0.01 |e|/bohr^3.

2.3 Microkinetic Model

Harmonic transition state theory was used to calculate all elementary rate constants of surface processes. Collision theory with a sticking coefficient of 1 was used to estimate the rate constants for adsorption processes. An H_2 partial pressure of 80 bar was used. A non-water 1,4-dioxane solvent is assumed, following a previous experimental study.[11] Water is commonly found in gas (hydrogen) streams and is also a product of the DODH reaction, which is approximated to be 0.1% of the H_2 partial pressure, i.e. 0.08 bar. The fugacities (partial pressures) of AE and DHF from our previous study were adopted, those being 2.95×10^{-3} and 0.965 bar, respectively.[14] More details of the microkinetic model are presented in the supporting information.

3. Results and discussions

3.1 DODH of AE over ReO_2(2O)/TiO_2(101)

We first performed a mechanistic study of the AE DODH over 6H-ReO_2(2O) which is the most stable species at 413K. The reaction starts from the physisorption of AE on 6H-ReO_2(2O). The breaking of the AE O-H bond is concomitant with the formation of a Re-O bond, which has an effective barrier of 1.42 eV (**Re-IM1→Re-IM2**). The formed Re-bonded OH reacts with a neighboring surface H of TiO_2(101), which forms a H_2O with a low barrier of 0.20 eV (**Re-IM2→Re-IM3**), followed by facile desorption of H_2O. The formed H vacancy on TiO_2(101) can be replenished by facile H migration on TiO_2 through a H_2O-assisted mechanism,[14, 34] whose energy barrier was estimated to be 0.42 eV (**Re-IM4→Re-IM5** in Fig. 4, see also Fig. S14). Here, we also assume that atomic H atoms are abundant and can be obtained by facile H_2

dissociation over an oxide supported metal cluster (e.g. Pd) and H spillover onto the oxide surface, following our previous study where we have shown that the energy barrier of H_2 dissociation on a Pd_4 cluster and H migration from Pd_4 to $CeO_2(111)$ are smaller than 0.1 eV in the presence of H_2O.[14] Here, we also assume that a $TiO_2(101)$-supported metal cluster serving the role of H_2 dissociation is distant from the $ReO_2(2O)$ species so that the property of $ReO_2(2O)$ is unaffected by the presence of the metal cluster. Since the atomic H is readily available at the active site through H_2 dissociation and H migration on $TiO_2(101)$, one H atom is equated with a 1/2 H_2 gas molecule (**Re-IM4**+1/2H_2(g)→**Re-IM5**) to replenish the hydrogen vacancy on $TiO_2(101)$ created due to the formation of the first H_2O molecule (for more details see the SI). The cleavage of another O-H bond requires overcoming a 0.35 eV barrier (**Re-IM5→Re-IM6**). Concomitant with the O-H breaking is the formation of the second H_2O by a Re-bonded OH and a surface hydrogen atom. The C-O bond breaking to form DHF has a low barrier of 0.16 eV (**Re-IM6→Re-IM7**), followed by a highly exergonic desorption of the physiosorbed DHF (**Re-IM7→Re-IM8**). The desorption of the second H_2O is also facile (**Re-IM8→Re-IM9**). The catalytic cycle is closed upon the replenishment of the hydrogen vacancy by surface H migration (**Re-IM9→Re-FS**). Since our calculations suggest that the first O-H cleavage on 6H-$ReO_2(2O)$ has a relatively high barrier when the reaction occurs in one elementary step, we also considered an alternative two-step pathway that allows for the cleavage of the first O-H bond (Fig. 5). A surface hydrogen can migrate to the $ReO_2(2O)$ species (**Re-IM1→Re-IM10**), followed by the cleavage of the first O-H bond of AE and the formation of a H_2O molecule (**Re-IM10→Re-IM11**). However, the effective barrier of the alternative process is calculated to be 1.50 eV (Fig. 5), higher than the above-mentioned pathway of 1.42 eV. Figure S15

illustrates the free energy profile of this reaction at 473K when the effective barrier is calculated to be 1.52 eV. Since the 5H-ReO_2(2O) species has essentially the same free energy with 6H-ReO_2(2O) at 473K (the difference is smaller than 0.01 eV, see Fig. 2a), we also calculated the reaction pathway on 5H-ReO_2(2O). The effective free energy barrier of the first O-H cleavage step is calculated to be 1.51 eV at 473K (see Fig. S16), suggesting that the free energy profile is essentially unaffected by a slightly lower hydrogen coverage on the TiO_2(101) surface. Throughout the reaction process, the first O-H cleavage step is found to be rate-controlling.

In our previous study of the DODH over ReO/CeO_2(111), the effective barrier of the first O-H bond breaking is 1.18 eV, i.e., lower than in the present case of 1.42 eV. To understand the noticeable difference in O-H bond breaking barriers, we note that the corresponding transition states of ReO/CeO_2(111)[14] and ReO_2(2O)/6H-TiO_2(101) have a ReOOH and ReO_2OH(2O) motif, respectively. The free energy of ReO is 0.06 eV lower than ReOOH at 413K when they are supported on CeO_2(111), as compared with an energy difference of 0.54 eV for ReO_2(2O) and ReO_2OH(2O) in the present study that ultimately originates from the higher reducibility of ceria relative to titania. Therefore, the more stabilized ReOOH of CeO_2(111) translates to a lower O-H bond breaking barrier.

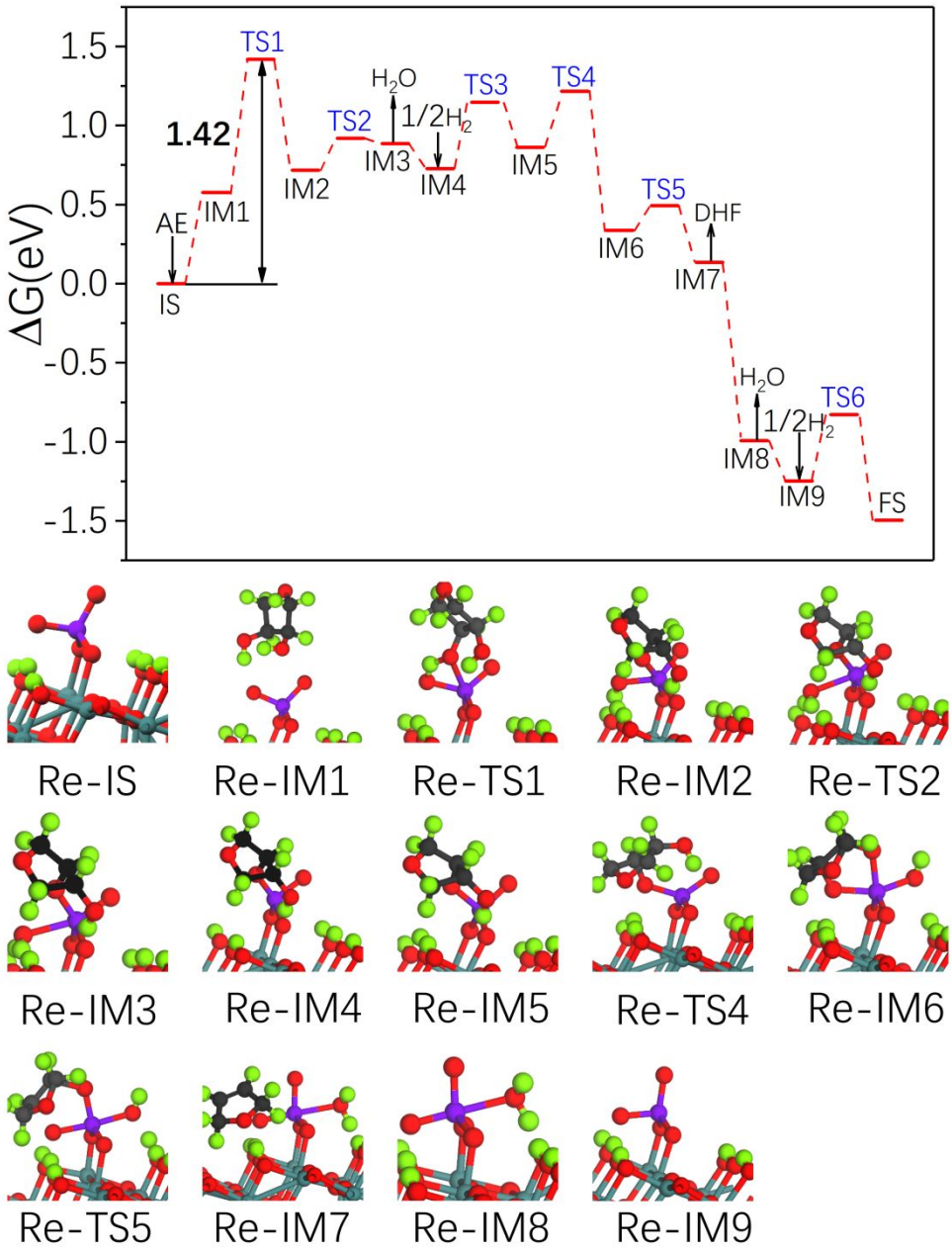

Fig. 4 Free energy profiles at 413K and structures of the initial, intermediate and transition states of the AE DODH reaction over ReO_2(2O)/6H-TiO_2(101). The **Re-** prefix is omitted in the energy profile for brevity. Carbon is shown in black. Other color codes are the same as in Fig. 1. Description of each elementary step and chemical formulas of initial/final and intermediate are presented in Table S1 and S2, respectively. The fugacities of all species are: H_2: 80 bar; H_2O: 0.08 bar; AE: 2.95×10^{-3} bar; DHF: 0.965 bar.

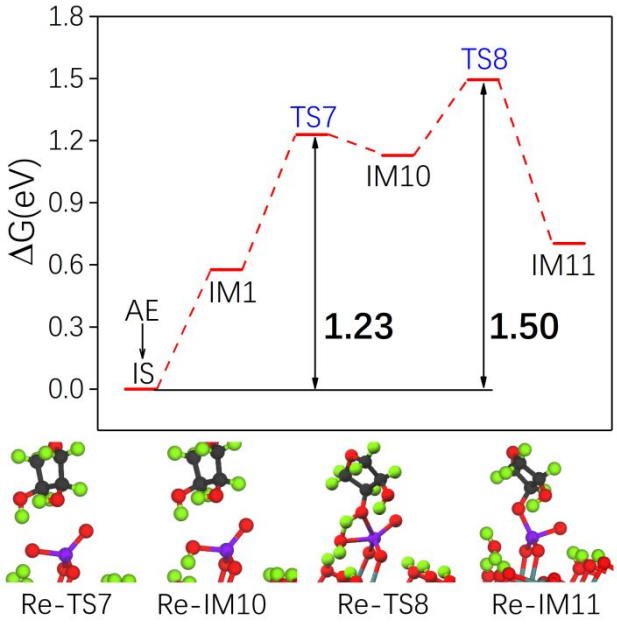

Fig. 5 Alternative two-step pathway of the first O-H breaking for the AE DODH reaction over ReO_2(2O)/6H-TiO_2(101). The fugacities of all species are: H_2, 80 bar; H_2O, 0.08 bar; AE, 2.95 × 10^{-3} bar.

3.2 DODH of AE over MoO_2(2O)/TiO_2(101)

We next investigated the DODH of AE catalyzed by 3H-MoO(2O). The free energy profile of the reaction at 473K is presented in Fig. 6, conditions at which 3H-MoO(2O) is the most stable species (Fig. 2b). A higher temperature of 473K is used here to present the free energy diagram owing to the relatively high effective barrier of the reaction while the free energy diagram at 413K is presented in Fig. S17. The first O-H cleavage has a relatively low effective barrier of 1.15 eV (**Mo-IM1→Mo-IM2**). The second O-H cleavage has a low barrier of 0.25 eV (**Mo-IM2→Mo-IM3**). After the facile desorption of a H_2O molecule (**Mo-IM3→Mo-IM4**), the extrusion of DHF has a comparatively high barrier of 1.51 eV (**Mo-IM4→Mo-IM5**). Next, physisorbed DHF desorbs without barrier (**Mo-IM5→Mo-IM6**). To complete the catalytic cycle, the formed MoO_2(2O) species needs to be reduced. As such, we allow a surface hydrogen atom to migrate to the oxygen of MoO_2(2O) (**Mo-IM6→Mo-IM7**), followed by facile

hydrogen migration (**Mo-IM7→Mo-IM8**) on TiO_2(101) to replenish the hydrogen vacancy. The formation of the second H_2O molecule has a relatively high effective barrier of 1.41 eV (**Mo-IM8→Mo-IM9**). Finally, after another hydrogen migration step (**Mo-IM9→Mo-IM10**) and desorption of H_2O, the catalytic cycle is closed. Throughout the reaction process, the DHF extrusion step is rate-limiting.

From the above reaction mechanism of AE DODH on ReO_2(2O)/6H-TiO_2(101) and MoO(2O)/3H-TiO_2(101), we have shown that the first O-H cleavage has a relatively high barrier on the former surface while the extrusion of DHF is difficult on the later. To understand the different activity of O-H cleavage, we plot the projected density of states (PDOSs) for the active oxygen in Fig. S18. The occupied PDOSs of oxygen accommodated on Mo is closer to the Fermi level than that of Re. Therefore, compared with the orbital of the oxygen on Re, the orbital of the oxygen on Mo are more likely to hybridize with the orbital of hydrogen of AE and hence the higher reactivity. For the DHF extrusion step, we note that **Re-IM6→Re-IM7** is exergonic by 0.22 eV, as compared with 0.08 eV for **Mo-IM4→Mo-IM5**. Also, **Re-IM6→Re-IM7** is accompanied by the formation of a H_2O, which is likely favorable for the extrusion of DHF.

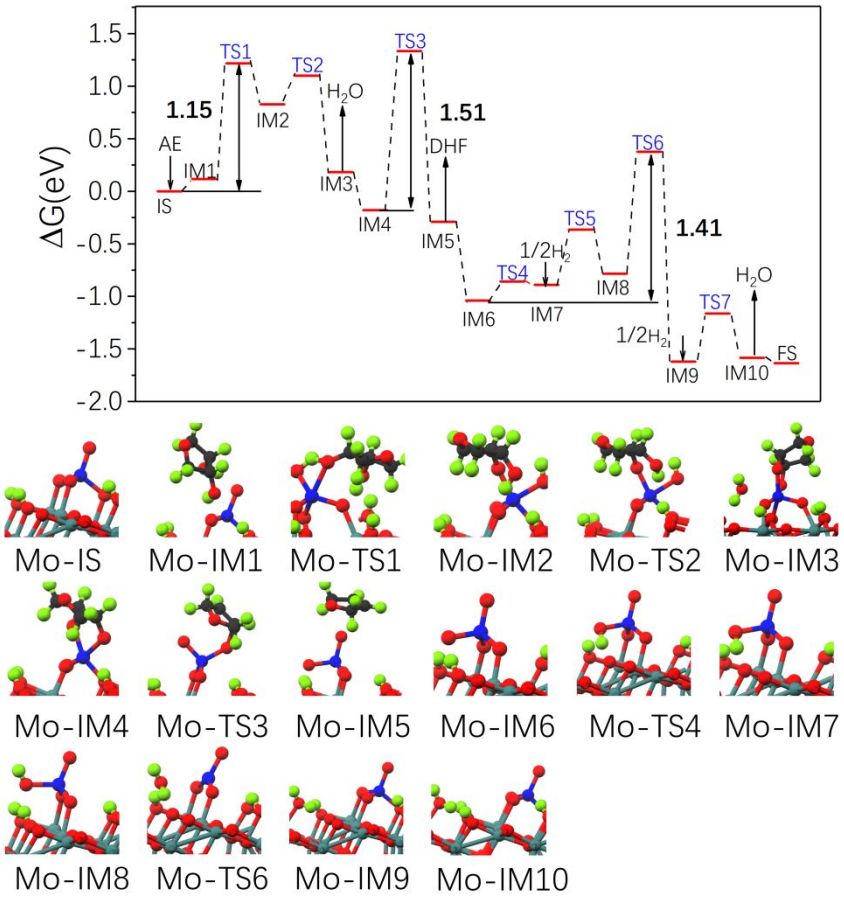

Fig. 6 Energy profiles and structures of initial and intermediate states of the AE DODH reaction over MoO(2O)/3H-TiO_2(101). The **Mo-** prefix is omitted in the energy profile for brevity. Description of each elementary step and chemical formulas of initial/final and intermediate are presented in Table S3 and S4, respectively. The fugacities of all species are: H_2, 80 bar; H_2O, 0.08 bar; AE, 2.95×10^{-3} bar; DHF, 0.965 bar.

3.3 Microkinetic modeling

We developed a microkinetic model for the DODH reaction to better understand the reaction kinetics of the ReO_2(2O)/6H-TiO_2(101) and MoO(2O)/3H-TiO_2(101) catalysts (details provided in the supporting information). At 413 K, the turnover frequency (TOF) for ReO_2(2O)/6H-TiO_2(101) was calculated to be 4.40×10^{-5}/s, noticeably lower than that of ReO/CeO_2(111) with a calculated TOF of 4.33×10^{-3}/s. [14] The calculated low reaction rate for ReO_2(2O)/TiO_2(101) echoes the previous experimental study of AE DODH over TiO_2-

supported ReO_x at 413K.[10] The TOF of the reaction on MoO(2O)/3H-TiO_2(101) was calculated to be 1.50×10^{-6}/s at 413K. A recent experiment has shown that TiO_2-supported MoO_x is active for the DODH of 1,2-decane diol at 473K and the TOF is 1.2×10^{-4}/s.[22] We therefore also calculated the TOFs of the two catalyst at 473K, which are 6.17×10^{-4}/s for ReO_2(2O)/6H-TiO_2(101) and 5.70×10^{-4}/s for MoO(2O)/3H-TiO_2(101), respectively. The reasonably high TOF of MoO(2O)/3H-TiO_2(101) at high temperature suggests that it is a promising low-cost replacement for the Re catalyst. The apparent activation energy for the two catalysts was found to be 0.74 and 1.66 eV, respectively (see Fig. 7), highlighting that the Mo-catalyst becomes active than the Re-catalyst at higher temperatures. A reaction order of 0 was obtained for H_2 for the reaction over ReO_2(2O)/6H-TiO_2(101) and MoO(2O)/3H-TiO_2(101), while the reaction orders for AE are 1 and 0.02 on the two catalysts.

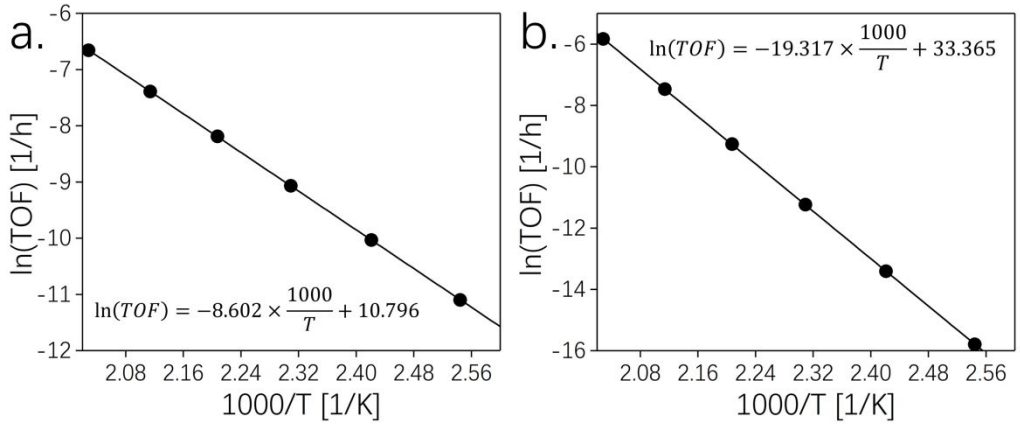

Fig. 7 Arrhenius plot for the AE DODH over ReO_2(2O)/6H-TiO_2(101) (**a**) and MoO (2O)/3H-TiO_2(101) (**b**) in the temperature range of 393−493 K.

4. Conclusions

We performed DFT calculations to investigate the DODH reaction of cis-1,4-anhydroerythritol (AE) over anatase TiO_2(101)-supported ReO_x and MoO_x. Using constrained thermodynamic calculations, the atomistic structures of ReO_x and MoO_x under reaction

conditions were identified to be ReO_2(2O)/6H-TiO_2 and MoO_2(2O)/3H-TiO_2, based on which we calculated the energy profiles of the AE DODH reaction. Surface hydrogen is indispensable for the reaction process. Here, we assumed that the source of atomic hydrogen is H_2 dissociation on a TiO_2(101) supported metal cluster and facile hydrogen migration on TiO_2(101) is enabled by H_2O. An effective overall free energy barrier of 1.42 eV and a calculated TOF of 4.40×10^{-5}/s at 413K (6.17×10^{-4}/s at 473K) suggest that the activity of ReO_2(2O)/6H-TiO_2(101) is low at low temperatures, which is consistent with experimental studies. The rate-limiting step is identified to be the first O-H cleavage step. For MoO(2O)/3H-TiO_2(101), we obtained an effective free energy barrier of 1.51 eV and a TOF of 5.70×10^{-4}/s at 473K (1.50×10^{-6}/s at 413K), whose rate-determining step was identified to be the DHF extrusion step. The reasonably high TOF at 473K for the reaction over MoO(2O)/3H-TiO_2(101) agrees with a recent experiment for the DODH of 1,2-decane diol on TiO_2-supported MoO_x performed at this temperature.

The low activity of ReO_2(2O)/TiO_2(101) in the present study and the reported high activity of ReO/CeO_2(111) underscores the importance of oxide support in determining the catalytic activity of supported single-atom species. The reasonably high activity of MoO(2O)/3H-TiO_2(101) suggests that it is potentially a promising low-cost DODH catalyst that can replace commonly used Re-based catalysts. Thus, this study sheds light on the design of low-cost DODH catalysts with high activity.

Author information

Corresponding Author

*E-mail for A.H.: heyden@cec.sc.edu.

Electronic supplementary information (ESI) available:

Gibbs free energies of $ReO_a(OH)_b(2O)/MoO_a(OH)_b(2O)$ species adsorbed on $TiO_2(101)$ at various hydrogen coverage; optimized structures of various $ReO_a(OH)_b(2O)$ and $MoO_a(OH)_b(2O)$ species on the fully-hydrogenated TiO_2 surface; energy profile of water-assisted H migration on anatase $TiO_2(101)$; free energy profiles at 473K of the reaction over $ReO_2(2O)/6H\text{-}TiO_2(101)$; free energy profiles of the first O-H cleavage of AE over $ReO_2(2O)/5H\text{-}TiO_2(101)$; free energy profiles at 413K of the reaction over $MoO(2O)/3H\text{-}TiO_2(101)$; projected density of states for the active oxygen; details of microkinetic model, coordinate files of optimized structures; description and chemical formulas of each elementary step for the reactions over $ReO_2(2O)/6H\text{-}TiO_2(101)$ and $MoO(2O)/3H\text{-}TiO_2(101)$.

Acknowledgments

We gratefully acknowledge financial support from the National Science Foundation (OIA-1632824). This research was performed using computing resources from EMSL (Ringgold ID 130367, Grant Proposal 49246), a DOE Office of Science User Facility sponsored by the Office of Biological and Environmental Research and the National Energy Research Scientific Computing Center, a DOE Office of Science User Facility supported by the Office of Science of the U.S. Department of Energy under Contract No. DE-AC02-05CH11231. This work was also supported by the South Carolina Smart State Center for Strategic Approaches to the Generation of Electricity (SAGE).

Competing financial interests

The authors declare no competing financial interest.

References

1. A. Corma, S. Iborra and A. Velty, *Chem. Rev.*, 2007, **107**, 2411-2502.
2. J. Q. Bond, D. M. Alonso, D. Wang, R. M. West and J. A. Dumesic, *Science*, 2010, **327**, 1110-1114.
3. A. D. Sutton, F. D. Waldie, R. Wu, M. Schlaf, L. A. Silks, 3rd and J. C. Gordon, *Nat Chem*, 2013, **5**, 428-432.
4. C. Li, X. Zhao, A. Wang, G. W. Huber and T. Zhang, *Chem Rev*, 2015, **115**, 11559-11624.
5. A. R. Petersen and P. Fristrup, *Chem. Eur. J.*, 2017, **23**, 10235-10243.
6. L. J. Donnelly, S. P. Thomas and J. B. Love, *Chemistry – An Asian Journal*, 2019, **14**, 3782-3790.
7. G. K. Cook and M. A. Andrews, *Journal of the American Chemical Society*, 1996, **118**, 9448-9449.
8. J. E. Ziegler, M. J. Zdilla, A. J. Evans and M. M. Abu-Omar, *Inorg. Chem.*, 2009, **48**, 9998-10000.
9. A. L. Denning, H. Dang, Z. Liu, K. M. Nicholas and F. C. Jentoft, *ChemCatChem*, 2013, **5**, 3567-3570.
10. N. Ota, M. Tamura, Y. Nakagawa, K. Okumura and K. Tomishige, *Angew Chem Int Ed* 2015, **54**, 1897-1900.
11. N. Ota, M. Tamura, Y. Nakagawa, K. Okumura and K. Tomishige, *ACS Catal.*, 2016, **6**, 3213-3226.
12. S. Tazawa, N. Ota, M. Tamura, Y. Nakagawa, K. Okumura and K. Tomishige, *ACS Catal.*, 2016, **6**, 6393-6397.

13. Y. Nakagawa, S. Tazawa, T. Wang, M. Tamura, N. Hiyoshi, K. Okumura and K. Tomishige, *ACS Catal.*, 2018, **8**, 584-595.

14. Y. J. Xi, W. Q. Yang, S. C. Ammal, J. Lauterbach, Y. Pagan-Torres and A. Heyden, *Catal. Sci. Technol.*, 2018, **8**, 5740-5752.

15. I. Ahmad, G. Chapman and K. M. Nicholas, *Organometallics*, 2011, **30**, 2810-2818.

16. C. Boucher-Jacobs and K. M. Nicholas, *ChemSusChem*, 2013, **6**, 597-599.

17. S. Liu, A. Senocak, J. L. Smeltz, L. Yang, B. Wegenhart, J. Yi, H. I. Kenttämaa, E. A. Ison and M. M. Abu-Omar, *Organometallics*, 2013, **32**, 3210-3219.

18. Y.-Y. Jiang, J.-L. Jiang and Y. Fu, *Organometallics*, 2016, **35**, 3388-3396.

19. L. Sandbrink, K. Beckerle, I. Meiners, R. Liffmann, K. Rahimi, J. Okuda and R. Palkovits, *ChemSusChem*, 2017, **10**, 1375-1379.

20. A. R. Petersen, L. B. Nielsen, J. R. Dethlefsen and P. Fristrup, *ChemCatChem*, 2018, **10**, 769-778.

21. L. Sandbrink, E. Klindtworth, H.-U. Islam, A. M. Beale and R. Palkovits, *ACS Catal.*, 2016, **6**, 677-680.

22. B. E. Sharkey, A. L. Denning, F. C. Jentoft, R. Gangadhara, T. V. Gopaladasu and K. M. Nicholas, *Catal. Today*, 2018, **310**, 86-93.

23. G. Kresse and J. Furthmuller, *Phys. Rev. B*, 1996, **54**, 11169.

24. G. Kresse and J. Furthmuller, *Comput. Mater. Sci.*, 1996, **6**, 15-50.

25. J. P. Perdew, K. Burke and M. Ernzerhof, *Phys. Rev. Lett.*, 1996, **77**, 3865.

26. P. E. Blochl, *Phys. Rev. B*, 1994, **50**, 17953-17979.

27. G. Kresse and D. Joubert, *Phys. Rev. B*, 1999, **59**, 1758-1775.

28. U. Aschauer and A. Selloni, *Physical Chemistry Chemical Physics*, 2012, **14**, 16595-16602.

29. H. J. Monkhorst and J. D. Pack, *Phys. Rev. B*, 1976, **13**, 5188.

30. S. Grimme, J. Antony, S. Ehrlich and H. Krieg, *J. Chem. Phys.*, 2010, **132**, 154104.

31. G. Henkelman, B. P. Uberuaga and H. Jonsson, *J. Chem. Phys.*, 2000, **113**, 9901-9904.

32. G. Henkelman and H. Jónsson, *J. Chem. Phys.*, 1999, **111**, 7010-7022.

33. A. Heyden, A. T. Bell and F. J. Keil, *J. Chem. Phys.*, 2005, **123**, 224101.

34. Y. Xi, Q. Zhang and H. Cheng, *J. Phys. Chem. C*, 2014, **118**, 494-501.

TOC Figure